




## Research Article

# Study on the Permeability of Weakly Cemented Sandstones

XianZhou Lyu <sup>1</sup>, Zenghui Zhao <sup>2</sup>, Xiaojie Wang,<sup>1</sup> and Weiming Wang <sup>1</sup>

<sup>1</sup>College of Architecture and Civil Engineering, Shandong University of Science and Technology, Qingdao 266590, China

<sup>2</sup>State Key Laboratory of Mining Disaster Prevention and Control Co-founded by Shandong Province and the Ministry of Science and Technology, Shandong University of Science and Technology, Qingdao 266590, China

Correspondence should be addressed to Zenghui Zhao; tgzyzh@163.com

Received 20 July 2018; Accepted 29 October 2018; Published 15 January 2019

Academic Editor: Mohammad Sarmadivaleh

Copyright © 2019 XianZhou Lyu et al. This is an open access article distributed under the Creative Commons Attribution License, which permits unrestricted use, distribution, and reproduction in any medium, provided the original work is properly cited.

Fractured rocks are a type of complex media that widely exist in various projects including energy, hydraulic, and underground space engineering, whose permeability properties are a hotspot in current rock mechanics domain. Aiming at investigating the seepage characteristics of the fracture surfaces in different rock strata, uniaxial compressive test and permeability test were performed on single-fracture homogenous and heterogeneous rocks. Specifically, rock's physical and mechanical parameters were measured in uniaxial tests while the initial width of the single fracture was determined through CT scanning. In combination with test results and the calculation model of the displacement of single-fracture heterogeneous rock under triaxial stress condition, the calculation formula of the permeability coefficient of single-fracture heterogeneous rock was derived. Results show that hydraulic pressure in the fracture can affect the permeability coefficient of the fractured rock. Hydraulic fracturing effect occurred with the increase of hydraulic pressure in the fracture, which then generates slight normal deformations of the rock masses on both two sides of the fracture surface, decreases the contact area in the fracture, and leads to the increases of both fracture width and permeability coefficient. For single-fracture rock, the lithological properties of the rock masses on both two sides of the fracture surface impose significant effects on the permeability coefficient. Under same hydraulic pressure and confining pressure, the permeability coefficient of single-fracture coarse sandstone is greatest, followed by that of single-fracture heterogeneous rock, and finally by single-fracture fine sandstone. Theoretical calculation results agree well with the test results, suggesting that the derived theoretical formula can adequately describe the variation tendencies of permeability coefficient with confining pressure and hydraulic pressure in the fracture.

## 1. Introduction

Seepage in fractured rocks can significantly affect construction stability in underground engineering [1–3], foundation engineering [4, 5], and rock-soil bodies on side slopes [6–8]. Generally, under long-term seismic load, construction-induced disturbance, and temperature effect, original fractures develop steadily and rock is gradually cut into several structural surfaces by the fracture network [9–11]. Under same stress, different rocks undergo different deformations because of the existence of the structural surfaces, and meanwhile, the formed structure surfaces act as main seepage channels of underground water. Pressure fluid mainly imposes action on rock skeleton via physical weakening and mechanical action, changes stress state in

the rock, rock shape, internal pores, and structural deformation of fractures, and finally affects seepage characteristics of fractured rocks.

Permeability coefficient and permeability tensor are two main parameters that are widely used for describing the permeability of fractured rocks [12–14], which are generally determined by theoretical calculation [15–18], field measurement [19], or laboratory test [20–23]. Currently, single-fracture parallel-plate hydraulic model [24] is most widely applied in theoretical estimation of seepage behaviors in fractured rocks, which assumes that the fracture has fixed ideal width. However, natural fractures are coarse to varying degrees, whose widths always change under external loading, thereby inducing the change of permeability coefficient. Existing research results demonstrate that the deformation

of fracture surfaces under loading is a major cause of the variation of permeability coefficient [25–31], while the permeability of rock heavily depends on the fracture properties. Therefore, stress effect and the change of fracture width should be taken into overall consideration in the calculation of permeability coefficient.

The fracture surface's geological properties including roughness and width are quite important for describing the fractured rock's permeability and mechanical properties [32, 33]. For a single-fracture rock, fracture width is related to normal stress on the fracture surface. The change of normal stress on the fracture surface can induce the change of fracture width and thus affect the permeability coefficient [34, 35]. With rapid development of modern optical technology, high-precision photoelectric instruments (computed tomography scanning and laser scanning) now are increasingly being applied in the scanning of fracture surface morphology and width. Bertels et al. [36] employed CT for measuring the fractures' width distribution, capillary force, relative permeability coefficient, and in situ saturability. By means of 3D laser scanning technique, Lanaro [37] measured surface morphology and width distribution of the fractures. Tatone and Grasselli [38] analyzed 2S roughness of the fractured rock using laser scanning. Tatone and Grasselli [39] used advanced topometric sensor (ATOS II, GOM mbH, Germany) for in situ large-size and laboratory small-scale digital processing. Zou et al. [40] examined the fracture surface of natural granite rock using laser and established the fracture model of roughness characterization and fluid flowing simulation. Wang et al. [41] acquired the roughness of the joint surface in the rocks using 3D-laser-scanning-based rock surface meter.

For a single-fracture heterogeneous rock, the rock masses on both two sides of the fracture exhibit different lithological properties or even significantly different physical and mechanical properties. Under the action of stress, the fracture's permeability coefficient is not only affected by hydraulic pressure and net confining pressure but also subjected to elastic moduli and Poisson's ratios of the rock masses on both two sides of the fracture. However, previous studies mainly focused on permeation rules of rocks with identical lithological properties on both two sides of the fracture (i.e., homogenous rocks), while the permeability of rocks with different lithological properties on both two sides (i.e., heterogeneous rocks) was poorly investigated. It is blind and unreliable to directly apply the permeability rules in homogenous rocks to heterogenous rocks. Therefore, for gaining in-depth knowledge of permeation evolutionary rules and permeability of single-fracture heterogeneous rock, this study first examined the permeation properties of single-fracture rock and single-fracture heterogeneous rock in the laboratory and determined the related physical/mechanical parameters. Next, based on fractured rock-displacement model, the theoretical calculation formula of the permeability coefficient of single-fracture heterogeneous rock (i.e., the rock with different lithological properties on both two sides of the fracture) was derived. Finally, by contrast to test results, accuracy and applicability of the developed calculation formula were validated.

## 2. Test Materials and Method

*2.1. Test Materials and Instrument.* Artificial cutting cracks are essentially different from the cracks in rock mass under natural loading in terms of openness, roughness, and coincidence of fracture surfaces. However, it is difficult to obtain rock samples containing fractures directly from the engineering site of weak cemented soft rock because of the poor mechanical behavior of low strength, poor cementation, and susceptibility to disturbance. Therefore, the artificial fracture method is used in this experiment. The present test specimens, with a size of  $\Phi 50 \times 100$  mm, were collected from the reconstruction and expansion project of a mine in Inner Mongolia, China, which mainly consist in weakly cemented coarse sandstone and weakly cemented fine sandstone. The uniaxial compressive strengths of the specimens are 31 MPa and 43 MPa, while the densities are  $2.24 \text{ g/cm}^3$  and  $2.45 \text{ g/cm}^3$ , respectively. In order to guarantee single-way seepage behaviors, all specimens should undergo vacuuming and saturated processing before the present permeation test. Using the numerically controlled machine tool, the specimens were then cut into semicylinders with bilateral symmetry and identical-geometry fracture surfaces. In accordance with the present test requirements, single-fracture coarse sandstone, single-fracture fine sandstone, and single-fracture heterogeneous rock specimen were prepared, as shown in Figure 1.

Microcomputer-controlled servo triaxial stress test system (TAW-2000M) was employed in this study, which can simultaneously apply confining pressure and hydraulic pressure. During the tests, the hydraulic pressure can be applied on pores from the bottom of the specimen, while the pore water flowed out from the top of the specimen, thereby forming osmotic pressure difference between two ends of the specimen. Figure 2 illustrates the loading process in the tests, during which both radial and axial stresses, strains, water discharge flow rate, and osmotic pressure difference between two ends can be measured in real time. Accordingly, the effects of confining pressure, osmotic pressure, and the geometric properties of the joint surface on the permeation rules in coarse fracture were examined so as to conclude fluid-solid coupling failure mechanisms of fractured soft rocks.

*2.2. Test Method.* In order to acquire normal stiffness coefficient, elastic modulus, and Poisson's ratio of the fracture surface in single-fracture rock, uniaxial compression test was first performed at a loading rate of 0.02 mm/min. After the splitting test, the specimens with high occlusion degrees were acquired, and the permeation test under different confining pressures and hydraulic pressures in the pores (i.e., osmotic pressure difference) was designed according to orthogonal experimental method. During the tests, the hydraulic pressure in the pores was 0.5 MPa, 1 MPa, 1.5 MPa, 3 MPa, and 5 MPa, respectively, which remained constant in each permeation test. Confining pressure was loaded in stepwise way, and net confining pressure (i.e., the difference between actual confining pressure and hydraulic pressure in the fracture) was set as 2 MPa, 4 MPa, 6 MPa, 10 MPa, and 15 MPa,

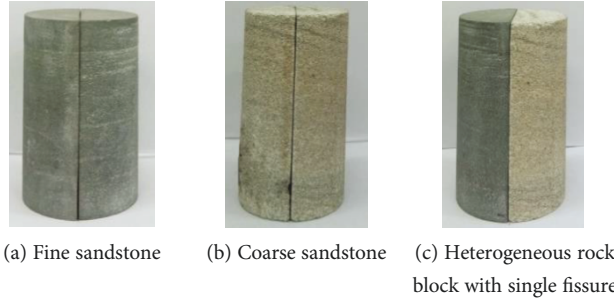


FIGURE 1: Single fissure rock block.

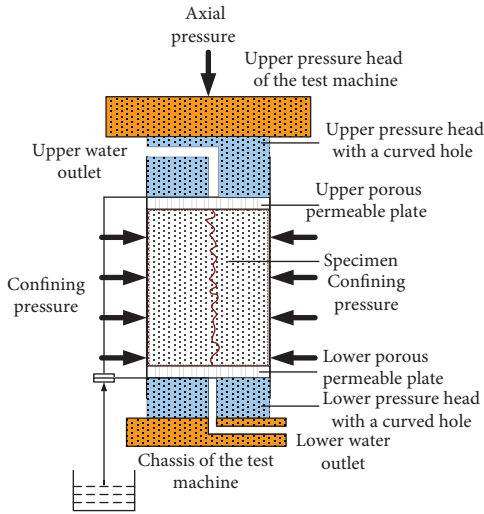


FIGURE 2: Sketch of fracture seepage test.

respectively. In each loading stage, the fracture hydraulic pressure should first be fixed and the test was carried out stage by stage by changing the confining pressure. Using water intake apparatus, the osmotic pressure was applied from the bottom of the specimen. After actual osmotic pressure reached stable, the flow within a certain period was measured and recorded, and next, the confining pressure/hydraulic pressure increased to the maximum in a stepwise way, and the flow at each level of confining pressure/hydraulic pressure was measured and recorded.

In order to guarantee unidirectional seepage in the fracture, both two sides of the longitudinal fracture in the specimen, both upper and lower ends of the circular, the joint between the specimen and the waterproof gasket, and the joint between upper and lower pressure heads were sealed by the silicone adhesive with a width of 5 mm and a thickness of 3 m. In addition, the specimen was spirally wrapped by a layer of plastic insulating tape from top to bottom so as to prevent water from flowing into the side of the specimen from the fracture and upper/lower joints. Figure 3 illustrates the detailed processing of the specimen.

Whether unidirectional seepage successfully occurred in the fractured rock can be judged below. Before the installation, the specimen should be placed in the shade until the

surface was dry, which can also facilitate the use of silicone adhesive. After the test, the specimen was taken out. As shown in Figure 4, the specimen in which unidirectional seepage achieved in the fracture exhibited dry surface but wet joint surface.

If the external surface of the specimen was wet, some water flowed through thermoplastic pipe and gap, suggesting an unsuccessful test; if oil was observed on the specimen surface or hydraulic pressure equaled to confining pressure in the test and cannot be successfully adjusted, thermoplastic pipe was broken down, i.e., the test also failed.

### 3. Geometrical Characteristics of the Joint Surface

Using CT scanning, the rock specimens were divided into complete specimens with equal-thickness slides and cutting specimens so as to acquire mean CT values before and after cutting and calculate the fracture width of the cutting specimen. According to the calculation formula of fracture width [42], the related measuring and calculating method was developed, as the principle displayed in Figure 5.

$$N = \frac{S(H_p^0 - H_p^1)}{L(1000 + H_p^0)}, \quad (1)$$

where  $N$  represents the fracture width,  $H_p^0$  denotes mean CT value of the designated area before the appearance of fracture,  $H_p^1$  denotes mean CT value of the designated area after the appearance of fracture,  $S$  denotes the area of the designated area,  $L$  denotes the fracture width, and air CT value was set as  $-1000$ .

According to Eq. (1), and above-described measuring principle, the rock specimen was divided into a lot of slides with uniform thickness along the longitudinal direction. CT scanning was performed on the specimens before and after cutting. Let  $L = L_1$ , Eq. (1) can be rewritten as

$$N = \frac{L_1 \times N_1 (H_p^0 - H_p^1)}{L_1 (1000 + H_p^0)}. \quad (2)$$

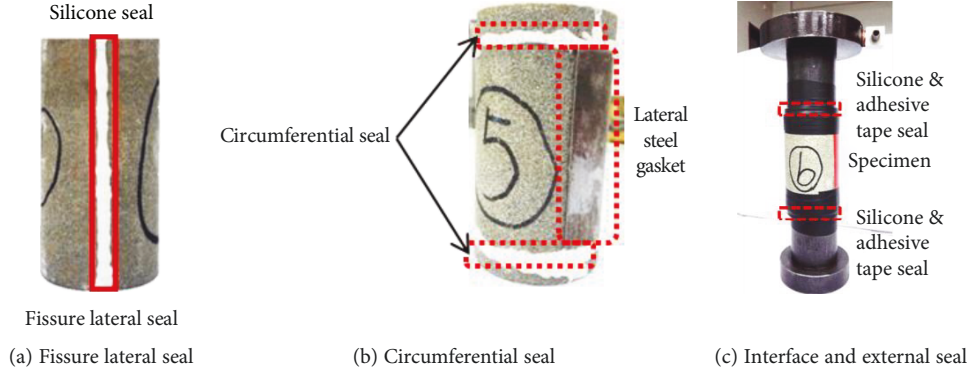


FIGURE 3: Treatment method of specimens for unidirectional fissure seepage.

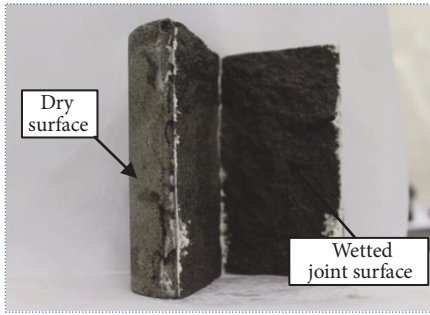


FIGURE 4: Surface characteristics of unidirectional fissure seepage.

After simplification, CT-based calculation formula of fracture width can be written as

$$N = \frac{N_1 (H_p^0 - H_p^1)}{(1000 + H_p^0)}. \quad (3)$$

By substituting mean CT number of longitudinal section of the original rock specimen ( $H_p^0$ ), mean CT number of longitudinal section of the rock specimen after cutting ( $H_p^1$ ), and the longitudinal width of the section ( $N_1$ ) into Eq. (3), the widths of the fractures on various longitudinal sections were calculated and averaged for acquiring the fracture width of the whole specimen. Using the simplified Eq. (3), the fracture width can be calculated only by measuring the width of unsplit specimen  $N_1$ , which can effectively reduce the accumulative error induced by manual measurement.

## 4. Test Results

### 4.1. Physical/Mechanical Parameters and Normal Stiffness.

The stress-strain curves of coarse and fine sandstones were acquired via uniaxial tests, and elastic moduli, Poisson's ratios, and post-peak deformation moduli of two kinds of rocks were approximately calculated, as the detailed results listed in Table 1.

Assuming  $\Delta d_t$  denotes the overall displacement of the fractured rock,  $\Delta d_f$  denotes the normal displacement of the fracture surface, and  $\Delta d_r$  denotes the normal displacement

of the rock, normal deformation of the fracture surface can be written as

$$\Delta d_f = \Delta d_t - \Delta d_r. \quad (4)$$

The normal displacement of single-fracture heterogeneous rock ( $\Delta d_r$ ) equals to the weighted average of the deformation of the coarse sandstone without structural surface ( $\Delta d_{rA}$ ) and the deformation of fine sandstone ( $\Delta d_{rB}$ ). Therefore,  $\sigma_n - \Delta d_f$  curves of single-fracture coarse sandstone, fine sandstone, and heterogeneous rock were plotted, as shown in Figure 6.

The normal stiffness coefficient of the fracture surface can be acquired by calculating the slope of  $\sigma_n - \Delta d_f$  curve as,

$$K_n = \frac{\partial \sigma_n}{\partial \Delta d_f}, \quad (5)$$

where  $K_n$  denotes the normal stiffness of the fracture surface.

Accordingly, normal stiffness coefficients of single-fracture coarse sandstone, fine sandstone, and heterogeneous rock equal to 18.11 GPa/cm, 45.67 GPa/cm, and 20.77 GPa/cm, respectively.

**4.2. Effects of Normal Stress and Osmotic Pressure on Permeability Coefficient.** Figure 7 displays the effect of osmotic pressure difference on permeability coefficient under certain normal stress. Apparently, when the normal stress was fixed, the permeability coefficient increases linearly with the osmotic pressure within a certain range. For different kinds of rocks, the relations can be described by the following expressions:

$$k = A\Delta P, \quad (6)$$

where  $k$  denotes the permeability coefficient, with a unit of cm/s,  $A$  denotes the straight slope and is correlated with some characteristics of the joint surface, and  $\Delta P$  denotes the osmotic pressure, with a unit of MPa.

With the increase of hydraulic pressure in the fractures, hydraulic fracturing effect was triggered and slight normal deformation on both two sides of the rock can be observed, which decreased the contact area in the fracture and induced



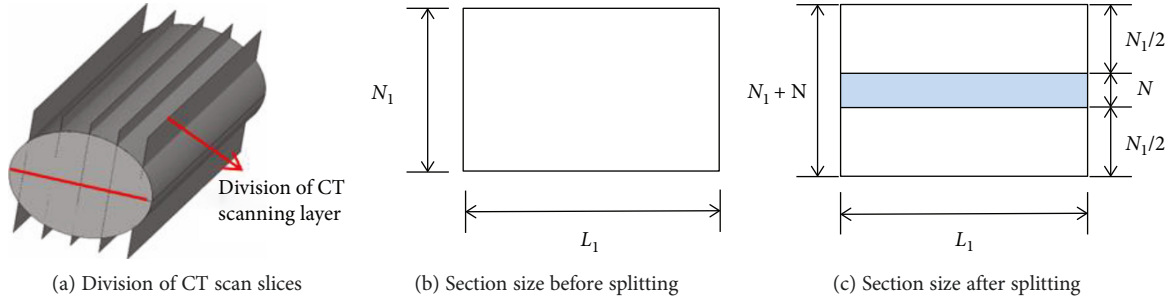


FIGURE 5: Schematic diagram of crack width calculation.

TABLE 1: Mechanical parameters of coarse sandstone and fine sandstone.

No.	$E/\text{GPa}$	$\mu$	$\sigma_c/\text{MPa}$
Coarse sandstone	15.084	0.18	31
Fine sandstone	25.765	0.21	43

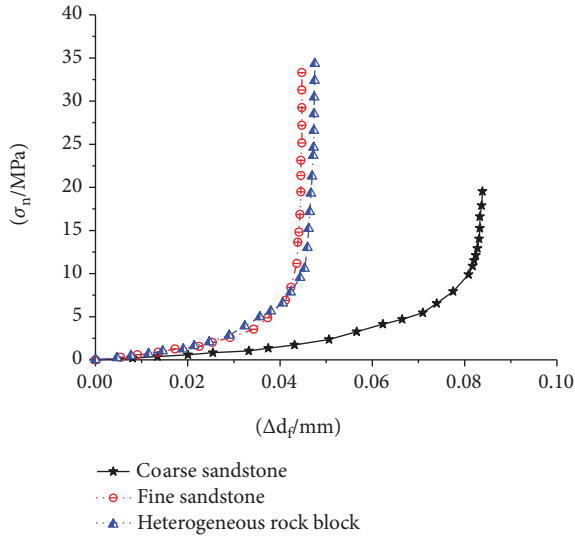


FIGURE 6: Normal deformation of fissure structure.

the increase of fracture width and permeability coefficient. Under a normal stress of below 10 MPa, because of the existence of hydraulic pressure in the fracture, the rock masses both two sides of the fracture were significantly deformed in normal direction, and therefore, the permeability of the fractured rock changed greatly. As the applied normal stress exceeded 10 MPa, hydraulic pressure in the fracture was relatively smaller compared with normal stress and the gas width only equaled to the residual gap width; because of the existence of high confining pressure, normal deformation of the rock on both two sides of the fracture surface was fairly limited under the action of hydraulic pressure in the fracture, thereby leading to slightly varying fracture width. Therefore, the effect of the hydraulic pressure in the fracture on the permeability coefficient of the fractured rock weakened with the increase of normal stress.

Figure 8 displays the relationship between normal stress and permeability coefficient under stepwise loading of hydraulic pressure when the normal stress was fixed. As normal stress increased, the permeability coefficient of the fractured rock decreased with varying amplitudes. When the normal stress was smaller than or equaled to 10 MPa, the permeability coefficient of the fractured rock dropped drastically with the increasing net confining pressure; when the normal stress exceeded 10 MPa, the permeability coefficient of the fractured rock dropped more gently with the increase of normal stress, which finally approached a constant value.

Through the above analysis, it is found that sandstones with different grain sizes have similar permeability characteristics, but the permeability coefficient varies greatly. The main reasons are as follows:

- (1) During the deformation of sandstone, the seepage path is the pore between grains. Therefore, the grain size has great influence on sandstone permeability. Under the same confining pressure, the smaller the grain size of sandstone, the closer the arrangement of grains, which causes smaller porosity and lower permeability. When the grain size is the same, the grain inside the sandstone is compacted with the increase of confining pressure, the porosity between the grains decreases, and the permeability decreases
- (2) On the other hand, although three kinds of single-fracture rocks are subjected to same effective normal stress and hydraulic pressure in the fracture, different normal additional deformations produce since the coarse/fine composite rock masses on both two sides of the fracture exhibit different elastic moduli, which lead to different variations of fracture widths. Therefore, the permeability coefficients of three types of rocks are different, and the properties of the rock masses on both two sides of the fracture surface in the fractured rock impose significant effects on the permeability coefficient of the fracture surface

## 5. Theoretical Calculation of Permeability Coefficient

5.1. Determination of Equivalent Mechanical Parameters. Sedimentary rock, as a layered rock mass, is often cut by

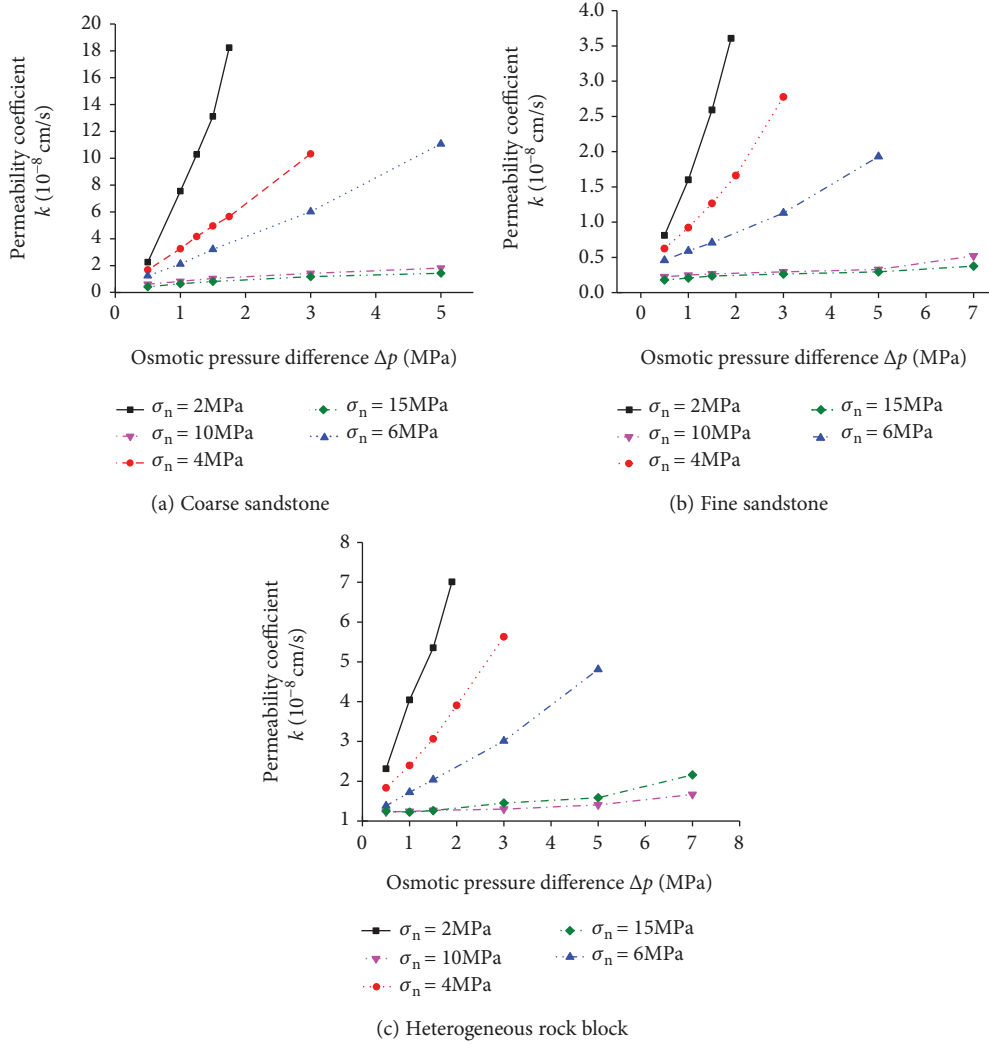


FIGURE 7: Relationship between permeability coefficient and osmotic pressure.

several parallel fractures. Therefore, the fracture of rock mass can be assumed as a parallel crack group for theoretical analysis. However, for fractured heterogeneous composite rock mass, the spacing and width of fractures are often unequal due to the lithological differences on both sides of the fractures. Thus, an equivalent continuum model of the single-fracture heterogeneous rock was presented in Figure 9. To be specific,  $\sigma_n$  represents the normal stress on the fracture structural surface. The rock masses on both two sides of the fracture surface can be treated as linear elastic bodies, whose thicknesses were denoted as  $a$  and  $b$ , respectively.  $K_n$  is the normal stiffness of fissure, and  $e$  denotes width. In addition, the surface opening was negligible.

Along the direction of  $\sigma$ -axis, both the structural surface and the rock mass produce normal displacement under the action of stress  $\sigma_n$ . The total displacement of rock blocks on both sides of fissure can be as written as

$$S_r = \frac{\sigma_n}{E_A} a + \frac{\sigma_n}{E_B} b, \quad (7)$$

where  $S_r$  represents the total normal displacement on both two sides of the fracture structural surface, while  $E_A$  and  $E_B$  denote the elastic moduli of the rock masses on both two sides of the fracture surface.

Displacement of the structural surface in normal direction can be written as

$$S_f = \frac{\sigma_n}{K_n}, \quad (8)$$

where  $S_f$  represents the normal displacement of the structural surface.

Total displacement of equivalent model in normal can be calculated as

$$S_t = \frac{\sigma_n}{E_t} l, \quad (9)$$

where  $E_t$  represents the equivalent deformation modulus of the single-fracture heterogeneous rock and  $l$  denotes total length of equivalent model which can also be expressed as  $l = a + b + e$ .

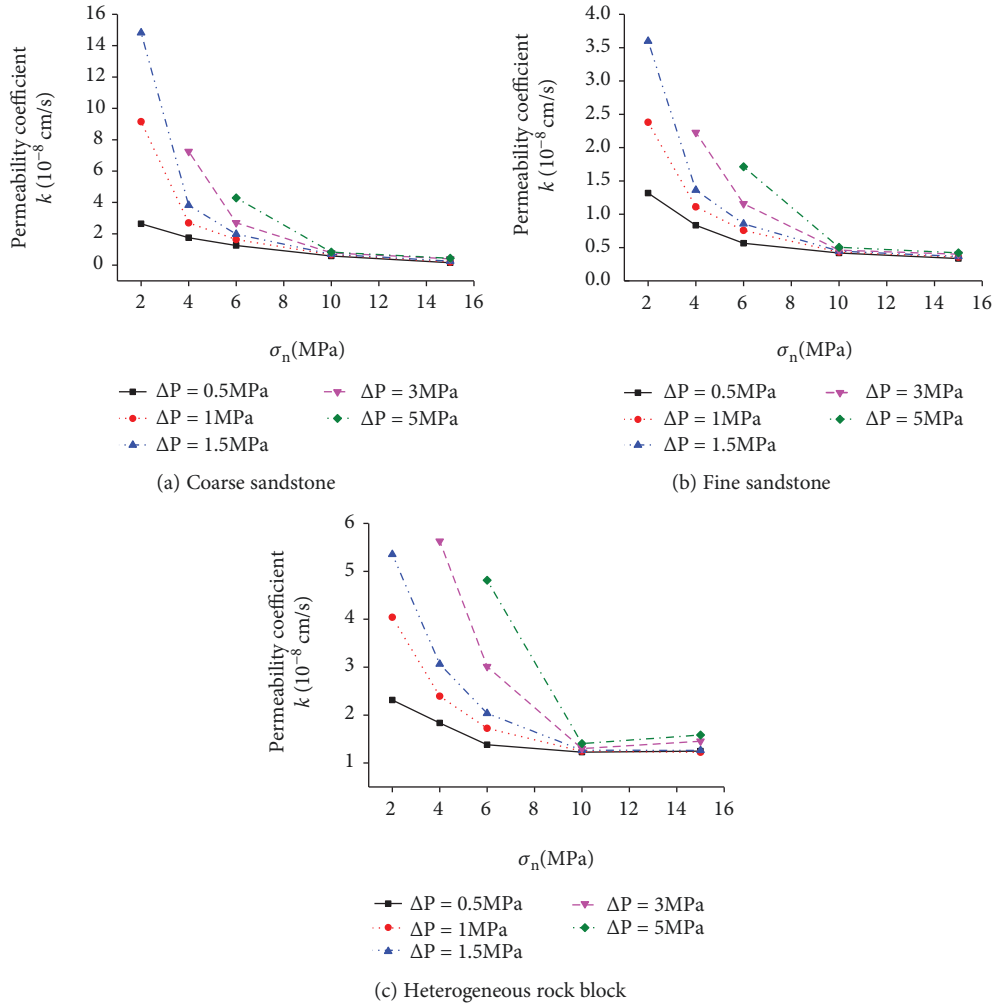


FIGURE 8: Relationship between permeability coefficient and normal stress.

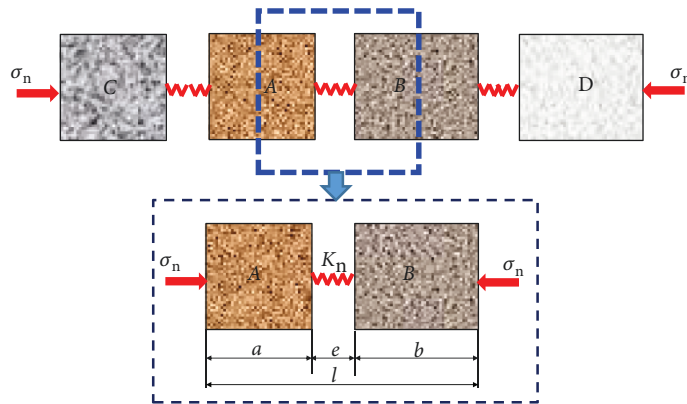


FIGURE 9: Equivalent continuum model of heterogeneous rock mass with single fissure.

Assuming that overall displacements of equivalent continuous model and original model remained unchanged, the following expression can be derived:

$$S_t = S_f + S_r. \tag{10}$$

By substituting Eqs. (7), (8), and (9) into Eq. (10), the following expression can be acquired:

$$\frac{\sigma_n}{E_t} l = \frac{\sigma_n}{K_n} + \frac{\sigma_n}{E_A} a + \frac{\sigma_n}{E_B} b. \tag{11}$$

Thus, equivalent deformation modulus of the single-fracture heterogeneous rock can be written as

$$E_t = \frac{K_n E_A E_B l}{E_A E_B + K_n E_B a + K_n E_A b}. \quad (12)$$

The strain of the fracture surface along the tangential direction should be neglected based on the model shown in Figure 9. Assuming that the strain of the single-fracture heterogeneous rock along the tangential direction equaled to the sum of the strains of the rock masses on both two sides of the fracture surface, then the following expression can be derived:

$$\mu_t \frac{\sigma_n}{E_t} = \mu_A \frac{\sigma_n}{E_A} + \mu_B \frac{\sigma_n}{E_B}, \quad (13)$$

where  $\mu_t$  denotes the equivalent Poisson's ratio of the single-fracture heterogeneous rock.  $\mu_A$  and  $\mu_B$  represent the Poisson's ratio of the rock masses on both two sides of the fracture surface, respectively.

By simplifying Eq. (13), the equivalent Poisson's ratio of the single-fracture heterogeneous rock can be written as

$$\mu_t = \frac{K_n (\mu_A E_B + \mu_B E_A) l}{E_A E_B + K_n E_B a + K_n E_A b}. \quad (14)$$

For single-fracture homogeneous rock, let  $E_A = E_B = E$  and  $\mu_A = \mu_B = \mu$ ; accordingly, deformation modulus and the Poisson's ratio of the single-fracture rock can be written as

$$E_t = \frac{K_n E l}{E + K_n (a + b)}, \quad (15)$$

$$\mu_t = \frac{\mu K_n l}{E + K_n (a + b)},$$

where  $E$  and  $\mu$  denote the elastic modulus and Poisson's ratio of the single-fracture homogenous rock, respectively.

**5.2. Permeability Coefficient of the Single-Fracture Rock.** For smooth single-fracture rocks, when the permeability of the rock masses on both two sides of the fracture were not taken into account, the permeability coefficient of the fractured rock can be written as [43–46]:

$$k = \frac{g e^2}{12\nu}, \quad (16)$$

where  $g$  denotes the gravitational acceleration ( $\text{m/s}^2$ ) and  $\nu$  denotes water's dynamic viscosity coefficient ( $\text{m}^2/\text{s}$ ).

Under the action of stress, the fracture width  $e$  will be changed, which can result in the change of permeability coefficient. According to the constitutive equation for fracture deformation [47], the fracture's deformation  $\Delta e$  can be written as

$$\Delta e = e_0 \left[ 1 - \exp \left( \frac{-\Delta \sigma_n}{K_n} \right) \right], \quad (17)$$

where

$$K_n = K_0 e_0, \quad (18)$$

$e_0$  denotes the initial fracture width of the single-fracture rock,  $K_n$  denotes the normal stiffness of the fracture surface,  $K_0$  denotes the initial normal stiffness coefficient of the fracture surface, and  $\Delta \sigma_n$  denotes the induced increment of normal stress on the fracture surface.

According to Eqs. (16), (17), and (18), the permeability coefficient of the single-fracture rock after the occurrence of displacement can be written as

$$k = \frac{g(e_0 - \Delta e)^2}{12\nu} = \frac{g e_0^2}{12\nu} \left[ \exp \left( -\frac{\Delta \sigma_n}{K_n} \right) \right]^2$$

$$= \frac{g e_0^2}{12\nu} [\exp(-\Delta \epsilon_n)]^2, \quad (19)$$

where  $\Delta \epsilon_n$  denotes the increment of normal strain of the fracture surface in the fractured rock.

**5.3. Derivation of the Calculation Formula of Permeability Coefficient of Single-Fracture Heterogeneous Rock.** Figure 10 presents the calculation model of the displacement of single-fracture heterogeneous rock under triaxial stress condition. A and B represent bedrocks with different lithological properties existed on two sides of the fracture surface.  $\Delta \sigma_x$ ,  $\Delta \sigma_y$ , and  $\Delta \sigma_z$  denote the normal stress increment of the fracture surface in  $x$ ,  $y$ , and  $z$  directions, respectively. Let the length of bedrocks and fracture be  $a$ ,  $b$ , and  $e$ .

According to the established calculation model, overall displacement of the single-fracture heterogeneous rock along  $x$  direction can be determined by

$$\Delta S_{tx} = (a + b + e) \Delta \epsilon_{tx}, \quad (20)$$

where  $\Delta \epsilon_{tx}$  denotes the total strain increments of single-fracture rock along the direction of  $x$ , respectively.

The total displacements of the rock masses on both two sides of the fracture can be calculated as

$$\Delta S_{rx} = a \Delta \epsilon_{Ax} + b \Delta \epsilon_{Bx}, \quad (21)$$

where  $\Delta \epsilon_{Ax}$  and  $\Delta \epsilon_{Bx}$  denote the strain increments of rock mass A and rock mass B along the direction of  $x$ , respectively.

Thus, fracture displacement can be calculated as

$$\Delta S_{fx} = \Delta S_{tx} - \Delta S_{rx} = (a + b + e) \Delta \epsilon_{tx} - (a \Delta \epsilon_{Ax} + b \Delta \epsilon_{Bx}). \quad (22)$$

Under tridirection compression, confining pressure and pore water pressure all cause compression deformation in rock blocks. Therefore, by taking into account the lithology of the single-fracture heterogeneous rock, hydraulic pressure and net confining pressure in the fracture, the strain increment of the single-fracture rock and the rock masses on



two sides of the fracture along the direction of  $x$  can be calculated as

$$\begin{cases} \Delta\varepsilon_{ix} = \frac{1}{E_t} [\Delta\sigma_x - \mu_t(\Delta\sigma_y + \Delta\sigma_z)], \\ \Delta\varepsilon_{Ax} = \frac{1}{E_A} [\Delta\sigma_x + \Delta P - \mu_A(\Delta\sigma_y + \Delta\sigma_z)], \\ \Delta\varepsilon_{Bx} = \frac{1}{E_B} [\Delta\sigma_x + \Delta P - \mu_B(\Delta\sigma_y + \Delta\sigma_z)], \end{cases} \quad (23)$$

where  $\Delta P$  denotes the increment of hydraulic pressure in the fracture.

By substituting Eq. (23) into Eq. (22), the fracture displacement can be derived:

$$\begin{aligned} \Delta S_{fx} = & \left( \frac{a+b+e}{E_t} - \frac{a}{E_A} - \frac{b}{E_B} \right) \Delta\sigma_x + \left[ \frac{a\mu_A}{E_A} + \frac{b\mu_B}{E_B} \right. \\ & \left. - \frac{(a+b+e)\mu_t}{E_t} \right] (\Delta\sigma_y + \Delta\sigma_z) - \left( \frac{a}{E_A} + \frac{b}{E_B} \right) \Delta P. \end{aligned} \quad (24)$$

The last item in Eq. (24) represents the additive deformation induced by hydraulic pressure in the fracture, which can also be written as

$$\Delta S_{Px} = \left( \frac{a}{E_A} + \frac{b}{E_B} \right) \Delta P. \quad (25)$$

It can be concluded that the hydraulic pressure in the fracture can compress the rock masses on both two sides of the fracture surface, thereby leading to increasing fracture width.

According to Eq. (25), the strain of the fracture along the direction of  $x$  can be written as

$$\begin{aligned} \Delta\varepsilon_{fx} = \frac{\Delta S_{fx}}{e} = & \left( \frac{a+b+e}{eE_t} - \frac{a}{eE_A} - \frac{b}{eE_B} \right) \Delta\sigma_x \\ & + \left[ \frac{a\mu_A}{eE_A} + \frac{b\mu_B}{eE_B} - \frac{(a+b+e)\mu_t}{eE_t} \right] (\Delta\sigma_y + \Delta\sigma_z) \\ & - \left( \frac{a}{eE_A} + \frac{b}{eE_B} \right) \Delta P. \end{aligned} \quad (26)$$

By substituting Eq. (26) to Eq. (19) and simplifying the equation, the permeability coefficient of the single-fracture heterogeneous rock can be written as

$$k = \frac{ge^2}{12\nu} \left\{ \exp \left[ \lambda_1 \Delta\sigma_x + \lambda_2 (\Delta\sigma_y + \Delta\sigma_z) + \lambda_3 \Delta P \right] \right\}^2, \quad (27)$$

where

$$\begin{aligned} \lambda_1 &= \frac{(aE_B + bE_A)E_t - (a+b+e)E_A E_B}{eE_A E_B E_t}, \\ \lambda_2 &= \frac{(a+b+e)\mu_t E_A E_B - (a\mu_A E_B + b\mu_B E_A)E_t}{eE_A E_B E_t}, \\ \lambda_3 &= \frac{aE_B + bE_A}{eE_A E_B}. \end{aligned} \quad (28)$$

The equivalent deformation modulus and equivalent Poisson's ratio of the single-fracture heterogeneous rock, denoted as  $E_t$  and  $\mu_t$ , can be calculated according to Eq. (12) and Eq. (14).

For single-fracture homogeneous rock and heterogeneous rock mass, the permeability coefficient can be calculated by Eq. (27). For single-fracture homogenous rock, let  $E_A = E_B = E$ ,  $\mu_A = \mu_B = \mu$ , and  $a = b = l$ . Then, the above three calculation coefficients can be simplified to

$$\begin{aligned} \lambda_1 &= \frac{lE_t - (l+e)E}{eEE_t}, \\ \lambda_2 &= \frac{(l+e)\mu_t E - l\mu E_t}{eEE_t}, \\ \lambda_3 &= \frac{l}{eE}. \end{aligned} \quad (29)$$

**5.4. Experimental Validation.** In the present tests, forces on the single-fracture rocks were simplified, during which only confining pressure and hydraulic pressure in the fracture were applied while no axial pressure was applied. In addition, only the effect of normal stress on the fracture surface of the rock was taken into account while the effect of shearing stress was not considered. Therefore, Figure 11 displays force condition on the rock specimen and the fracture surface,

$$\begin{cases} \Delta\sigma_z = 0, \\ \Delta\sigma_x = \Delta\sigma_y = \Delta\sigma_n, \end{cases} \quad (30)$$

in which  $\Delta\sigma_n$  denotes the net confining pressure (i.e., the difference between confining pressure  $\sigma$  and the hydraulic pressure  $P$  in the fracture).

By substituting Eq. (30) into Eq. (24), the following expression can be derived:

$$\begin{aligned} \Delta S_{fx} = & \left[ \frac{(1-\mu_t)(D+e)}{E_t} + \frac{(\mu_A E_B + \mu_B E_A)D - (E_B + E_A)D}{2E_A E_B} \right] \Delta\sigma_n \\ & - \frac{(E_B + E_A)D}{2E_A E_B} \Delta P, \end{aligned} \quad (31)$$

where  $D$  is the diameter of the specimen.

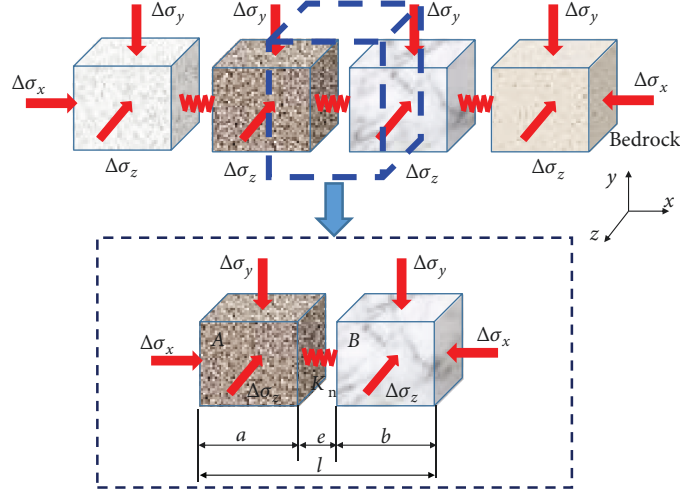


FIGURE 10: Displacement calculation model of heterogeneous rock mass with single fissure under three-direction stress condition.

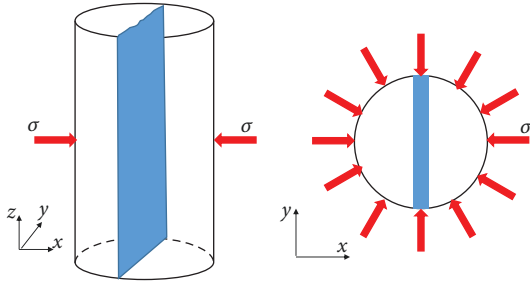


FIGURE 11: Sketch of rock specimen and fissure structure.

At the beginning of test,  $\Delta\sigma_n = 0$  and  $e = 0$ . According to Eq. (31), the following expression can be acquired:

$$\Delta S_{fx} = -\frac{(E_B + E_A)D}{2E_A E_B} \Delta P. \quad (32)$$

Accordingly, original displacement of the fracture in the single-fracture rock, i.e., initial fracture width, mainly depended on the hydraulic pressure in the fracture, which also increased with the increasing hydraulic pressure. As the hydraulic pressure increased with a constant, overall displacement of the fracture can be written as

$$S_{fx} = -\frac{(E_B + E_A)D}{2E_A E_B} P, \quad (33)$$

where  $P$  is the constant value that can be reached after the hydraulic pressure increases.

The absolute value of Eq. (33) equaled to the initial fracture width:

$$e = |S_{fx}| = \frac{(E_B + E_A)D}{2E_A E_B} P. \quad (34)$$

During the tests, the hydraulic pressure in the fracture was applied and remained unchanged until it reached a certain value; next, the confining pressure was changed. At that

moment,  $\Delta P = 0$ , and the initial fracture width is  $e$ . Therefore, the validation formula of the permeability coefficient of single-fracture heterogeneous rock can be described as

$$k = \frac{ge^2}{12\nu} \exp [2(\lambda_1 + \lambda_2)\Delta\sigma_n], \quad (35)$$

where

$$\lambda_1 = \frac{(E_B + E_A)DE_t - 2(D + e)E_A E_B}{2eE_A E_B E_t}, \quad (36)$$

$$\lambda_2 = \frac{2(D + e)\mu_t E_A E_B - (\mu_A E_B + \mu_B E_A)DE_t}{2eE_A E_B E_t}.$$

For single-fracture homogenous rock (i.e., the rock masses on both two sides of the rock had same lithological properties), the coefficient expressions can be written as

$$\lambda_1 = \frac{DE_t - (D + e)E}{eEE_t}, \quad (37)$$

$$\lambda_2 = \frac{(D + e)\mu_t E - \mu DE_t}{eEE_t}.$$

In the present test, the permeability coefficient of the rock specimen was calculated below based on Darcy law:

$$k = \frac{qL\gamma_w}{\Delta PA} \times 10^{-7}, \quad (38)$$

where  $k$  denotes the permeability coefficient of the rock specimen (cm/s),  $q$  denotes the seepage flow rate in the rock specimen (mL/s),  $L$  denotes the length of the specimen (cm),  $A$  denotes the cross-sectional area of the rock specimen (cm<sup>2</sup>),  $\Delta P$  denotes the osmotic pressure difference on both two sides of the rock specimen (MPa), and  $\gamma_w$  denotes water's unit weight (kN/m<sup>3</sup>).

As stated above, only the effect of normal stress on the fracture was taken into account while the effect of shearing

TABLE 2: Calculation of various parameters and permeability coefficient of fractured rock mass.

Classification	$E/\text{GPa}$	$\mu$	$D/\text{cm}$	$P/\text{MPa}$	$K_n/\text{GPa}\cdot\text{cm}^{-1}$	$E_t/\text{GPa}$	$\mu_t$	$e/\text{mm}$	Net confining pressure/MPa
Coarse sandstone	15.08	0.18	5.0	2	18.11	9.051	0.108	0.17	2
									4
									6
									10
									15
Fine sandstone	25.77	0.21	5.0	2	45.67	17.755	0.145	0.097	2
									4
									6
									10
									15
Heterogeneous rock mass	—	—	5.0	2	20.77	10.562	0.111	0.14	2
									4
									6
									10
									15

stress was neglected. According to the theoretical calculation formulas, Eq. (35), the theoretical permeability coefficients were calculated. By taking the condition under a hydraulic pressure of 2 MPa as the example, the derived theoretical formula of the permeability coefficient of the single-fracture rock was experimentally validated. Table 2 lists parameter results of the fractured rocks.

Figure 12 compares the calculated permeability coefficients of different single-fracture fractured rock specimens and the measured values. The theoretical calculated results fit well with the test data. Specifically, these two sets of values were within a same order of magnitude and exhibited almost identical variation tendencies with the net confining pressure. Therefore, the derived theoretical calculation formula of permeability coefficient of the fractured rock was verified to be accurate and applicable. The application condition of Eq. (35) is fixed hydraulic pressure in the fracture but varying confining pressure. When the hydraulic pressure in the fracture and the confining pressure change simultaneously, the permeability coefficient of the fractured rock should be calculated according to Eq. (27). Because of the restriction in experimental condition, accuracy and applicability of Eq. (27) should be further experimentally validated in future studies.

## 6. Conclusions

In this paper, we analyzed the seepage characteristics of weakly cemented sandstone with different granularity based on experimental and theoretical methods. A theoretical calculation formula of permeability coefficient of single-fracture heterogeneous rock (i.e., the rock masses on both two sides of the fracture differed in lithology) was derived based on fractured rock-displacement model. The theoretical results and experimental results were then compared. The main conclusions are drawn as follows:

- (1) As hydraulic pressure in the fracture increases, hydraulic fracturing effect is triggered, thereby generating slight normal deformation of the rock masses on both two sides of the fracture surface and decreasing the contact area in the fracture. Accordingly, both fracture width and permeability coefficient increase. As the applied normal stress exceed to a certain value, hydraulic pressure in the fracture is relatively smaller compared with normal stress and only residue fracture can be observed (i.e., the residual fracture width can be regarded to the fracture width); because of the existence of high confining pressure, limited normal deformation of the rock masses on both two sides of the fracture surface is generated under hydraulic action, and the fracture width slightly varies. Therefore, under a high normal stress, hydraulic pressure in the fracture imposes slight effect on the permeability coefficient of the fractured rock
- (2) The permeability coefficients of different types of fractured rocks all drop with the increasing normal stress but exhibit different magnitudes. When the normal stress is smaller than or equaled to 10 MPa, the permeability coefficient drops rapidly with the increase of net confining pressure. As the applied normal stress increase to over 10 MPa, the permeability coefficient drops more gently and finally approached to a constant
- (3) The lithological properties of the rock masses on both two sides of the fracture surface significantly affect the permeability coefficient of single-fracture rock. Under identical hydraulic pressure and confining pressure, the permeability coefficient of single-fracture coarse sandstone is greatest, followed by that of single-fracture heterogeneous rock, and

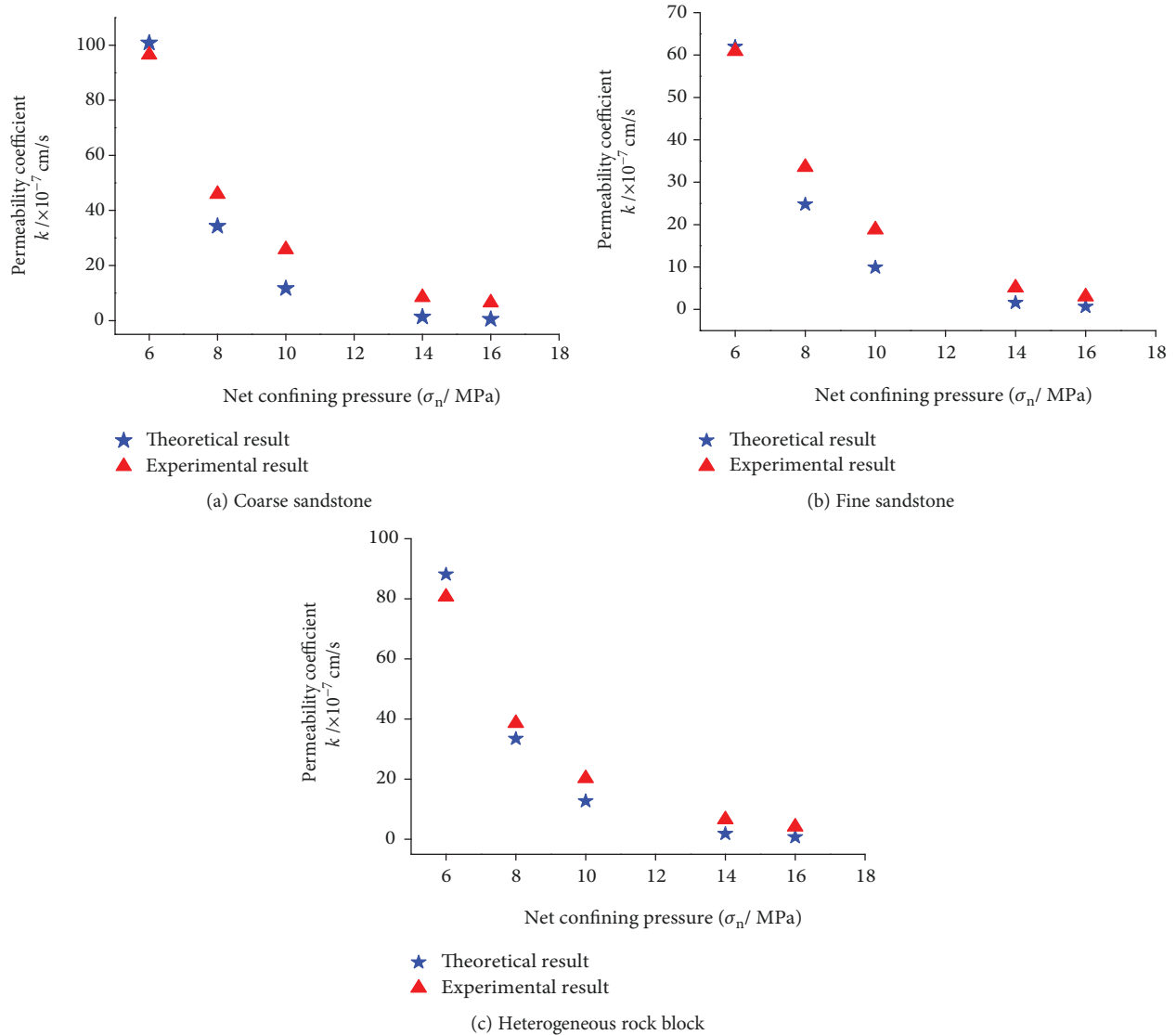


FIGURE 12: Comparison of calculated values and experimental values of permeability coefficient.

the permeability coefficient of single-fracture fine sandstone is lowest

- (4) All the parameters in the calculation model can be experimentally measured, which are independent of empirical and semiempirical settings. Moreover, theoretical calculation results of permeability coefficient fit well with the test data, which confirmed the variation tendencies of permeability coefficient and stress on the fracture surface

### Data Availability

The data used to support the findings of this study are available from the corresponding author upon request.

### Conflicts of Interest

The authors declare that they have no conflicts of interest.

### Acknowledgments

This paper was supported by the National Natural Science Foundation of China (nos. 51774196, 41472280), China Postdoctoral Science Foundation (no. 2016M592221), and SDUST Young Teachers Teaching Talent Training Plan (no. BJRC20160501).

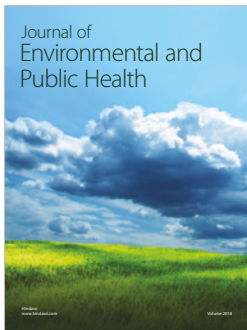
### References

- [1] D. Or, M. Tuller, and R. Fedors, "Seepage into drifts and tunnels in unsaturated fractured rock," *Water Resources Research*, vol. 41, no. 5, 2005.
- [2] K. Bian, M. Xiao, and J. Chen, "Study on coupled seepage and stress fields in the concrete lining of the underground pipe with high water pressure," *Tunnelling and Underground Space Technology*, vol. 24, no. 3, pp. 287–295, 2009.
- [3] Y. Li, Y. Chen, Q. Jiang, R. Hu, and C. Zhou, "Performance assessment and optimization of seepage control system: a

- numerical case study for Kala underground powerhouse,” *Computers and Geotechnics*, vol. 55, no. 2, pp. 306–315, 2014.
- [4] S. E. Cho, “Probabilistic analysis of seepage that considers the spatial variability of permeability for an embankment on soil foundation,” *Engineering Geology*, vol. 133–134, no. 3, pp. 30–39, 2012.
- [5] Y. Xiang, L. Wang, S. Wu, H. Yuan, and Z. Wang, “Seepage analysis of the fractured rock mass in the foundation of the main dam of the Xiaolangdi water control project,” *Environmental Earth Sciences*, vol. 74, no. 5, pp. 4453–4468, 2015.
- [6] L. Lam and D. G. Fredlund, “Saturated-unsaturated transient finite element seepage model for geotechnical engineering,” *Advances in Water Resources*, vol. 7, no. 3, pp. 132–136, 1984.
- [7] T. M. H. Le, D. Gallipoli, M. Sánchez, and S. Wheeler, “Stability and failure mass of unsaturated heterogeneous slopes,” *Canadian Geotechnical Journal*, vol. 52, no. 11, pp. 1747–1761, 2015.
- [8] A. Srivastava, G. L. S. Babu, and S. Haldar, “Influence of spatial variability of permeability property on steady state seepage flow and slope stability analysis,” *Engineering Geology*, vol. 110, no. 3–4, pp. 93–101, 2010.
- [9] H. O. Ghaffari, M. Sharifzadeh, and M. Fall, “Analysis of aperture evolution in a rock joint using a complex network approach,” *International Journal of Rock Mechanics and Mining Sciences*, vol. 47, no. 1, pp. 17–29, 2010.
- [10] Y. Zhao, L. Zhang, W. Wang, J. Tang, H. Lin, and W. Wan, “Transient pulse test and morphological analysis of single rock fractures,” *International Journal of Rock Mechanics and Mining Sciences*, vol. 91, pp. 139–154, 2017.
- [11] X. Lyu, Z. Zhao, Q. Ma, X. Wang, and X. Gao, “2D semimodel of full-section anchorage in thick soft rock roadway,” *Shock and Vibration*, vol. 2018, Article ID 9853853, 15 pages, 2018.
- [12] J. H. Li, L. M. Zhang, Y. Wang, and D. G. Fredlund, “Permeability tensor and representative elementary volume of saturated cracked soil,” *Canadian Geotechnical Journal*, vol. 46, no. 8, pp. 928–942, 2009.
- [13] P. Pérez-Flores, G. Wang, T. M. Mitchell et al., “The effect of offset on fracture permeability of rocks from the Southern Andes Volcanic Zone, Chile,” *Journal of Structural Geology*, vol. 104, pp. 142–158, 2017.
- [14] S. A. Shapiro, P. Audigane, and J. J. Royer, “Large-scale in situ permeability tensor of rocks from induced microseismicity,” *Geophysical Journal International*, vol. 137, no. 1, pp. 207–213, 1999.
- [15] G. H. Chen, K. H. Xie, Y. F. Cheng, and Y. Xu, “Analytical solution for consolidation of sand-drained ground considering variation of permeability coefficient in smeared zone,” *Journal of Zhejiang University (Engineering Science)*, vol. 45, no. 4, pp. 665–670, 2011.
- [16] M. Oda, “Permeability tensor for discontinuous rock masses,” *Géotechnique*, vol. 35, no. 4, pp. 483–495, 1985.
- [17] Z. Q. Wei, P. Egger, and F. Descoedres, “Permeability predictions for jointed rock masses,” *International Journal of Rock Mechanics and Mining Sciences & Geomechanics Abstracts*, vol. 32, no. 3, pp. 251–261, 1995.
- [18] G. Wang, X. Zhang, Y. Jiang, X. Wu, and S. Wang, “Rate-dependent mechanical behavior of rough rock joints,” *International Journal of Rock Mechanics and Mining Sciences*, vol. 83, pp. 231–240, 2016.
- [19] W. Yi and E. Wang, “Experimental research on measurement of permeability coefficient on the fault zone under coal mine in situ,” *Arabian Journal of Geosciences*, vol. 9, no. 4, p. 253, 2016.
- [20] M. D. Ingraham, S. J. Bauer, K. A. Issen, and T. A. Dewers, “Evolution of permeability and Biot coefficient at high mean stresses in high porosity sandstone,” *International Journal of Rock Mechanics and Mining Sciences*, vol. 96, pp. 1–10, 2017.
- [21] W. Z. Liu, M. L. Shi, and L. C. Miao, “Experimental study of permeability coefficient of natural saturated clay and its prediction model,” *Rock and Soil Mechanics*, vol. 34, no. 9, pp. 2501–2507, 2013.
- [22] N. He, N. S. Chen, Y. H. Zhu, J. Y. Yang, and C. L. Yang, “Experiment study of fractal feature and relationship between fractal dimension and permeability coefficient of gravelly soil in debris flow source area,” *Rock and Soil Mechanics*, vol. 35, no. 9, pp. 2543–2548, 2014.
- [23] R. Olsson and N. Barton, “An improved model for hydromechanical coupling during shearing of rock joints,” *International Journal of Rock Mechanics and Mining Sciences*, vol. 38, no. 3, pp. 317–329, 2001.
- [24] G. M. Lomize, *Flow in Fractured Rocks*, Gosemergoizdat, Moscow, Russia, 1951.
- [25] N. Barton, S. Bandis, and K. Bakhtar, “Strength, deformation and conductivity coupling of rock joints,” *International Journal of Rock Mechanics and Mining Sciences & Geomechanics Abstracts*, vol. 22, no. 3, pp. 121–140, 1985.
- [26] G. Cammarata, C. Fidelibus, M. Cravero, and G. Barla, “The hydro-mechanically coupled response of rock fractures,” *Rock Mechanics and Rock Engineering*, vol. 40, no. 1, pp. 41–61, 2007.
- [27] A. F. Gangi, “Variation of whole and fractured porous rock permeability with confining pressure,” *International Journal of Rock Mechanics and Mining Sciences & Geomechanics Abstracts*, vol. 15, no. 5, pp. 249–257, 1978.
- [28] M. Souley, P. Lopez, M. Boulon, and A. Thoraval, “Experimental hydromechanical characterization and numerical modelling of a fractured and porous sandstone,” *Rock Mechanics and Rock Engineering*, vol. 48, no. 3, pp. 1143–1161, 2015.
- [29] J. Zhang, W. B. Standifird, J. C. Roegiers, and Y. Zhang, “Stress-dependent fluid flow and permeability in fractured media: from lab experiments to engineering applications,” *Rock Mechanics and Rock Engineering*, vol. 40, no. 1, pp. 3–21, 2007.
- [30] Z. Zhao, Q. Ma, S. Chen, H. Ma, and X. Gao, “Prediction model of failure zone in roadway sidewall considering the lithologic effect of rock formation,” *Mathematical Problems in Engineering*, vol. 2018, Article ID 9627564, 12 pages, 2018.
- [31] D. Vogler, R. R. Settgest, C. Annavarapu, C. Madonna, P. Bayer, and F. Amann, “Experiments and simulations of fully hydro-mechanically coupled response of rough fractures exposed to high-pressure fluid injection,” *Journal of Geophysical Research: Solid Earth*, vol. 123, no. 2, pp. 1186–1200, 2018.
- [32] Y. Li, “Unsaturated hydraulic properties of rock fractures and their variation law,” *Rock and Soil Mechanics*, vol. 37, no. 8, pp. 2254–2262, 2016.
- [33] T. Zhou, S. Zhang, L. Yang, X. Ma, Y. Zou, and H. Lin, “Experimental investigation on fracture surface strength softening induced by fracturing fluid imbibition and its impacts on flow conductivity in shale reservoirs,” *Journal of Natural Gas Science and Engineering*, vol. 36, pp. 893–905, 2016.



- [34] M. J. Boulon, A. P. S. Selvadurai, H. Benjelloun, and B. Feuga, "Influence of rock joint degradation on hydraulic conductivity," *International Journal of Rock Mechanics and Mining Sciences & Geomechanics Abstracts*, vol. 30, no. 7, pp. 1311–1317, 1993.
- [35] T. H. Yang, P. Jia, W. H. Shi, P. T. Wang, H. L. Liu, and Q. L. Yu, "Seepage-stress coupled analysis on anisotropic characteristics of the fractured rock mass around roadway," *Tunnelling and Underground Space Technology*, vol. 43, no. 7, pp. 11–19, 2014.
- [36] S. P. Bertels, D. A. Dicarolo, and M. J. Blunt, "Measurement of aperture distribution, capillary pressure, relative permeability, and in situ saturation in a rock fracture using computed tomography scanning," *Water Resources Research*, vol. 37, no. 3, pp. 649–662, 2001.
- [37] F. Lanaro, "A random field model for surface roughness and aperture of rock fractures," *International Journal of Rock Mechanics and Mining Sciences*, vol. 37, no. 8, pp. 1195–1210, 2000.
- [38] B. S. A. Tatone and G. Grasselli, "A new 2D discontinuity roughness parameter and its correlation with JRC," *International Journal of Rock Mechanics and Mining Sciences*, vol. 47, no. 8, pp. 1391–1400, 2010.
- [39] B. S. A. Tatone and G. Grasselli, "An investigation of discontinuity roughness scale dependency using high-resolution surface measurements," *Rock Mechanics and Rock Engineering*, vol. 46, no. 4, pp. 657–681, 2013.
- [40] L. Zou, B. G. Tarasov, A. V. Dyskin, D. P. Adhikary, E. Pasternak, and W. Xu, "Physical modelling of stress-dependent permeability in fractured rocks," *Rock Mechanics and Rock Engineering*, vol. 46, no. 1, pp. 67–81, 2013.
- [41] W. X. Wang, W. H. Sui, B. Faybishenko, and W. T. Stringfellow, "Permeability variations within mining-induced fractured rock mass and its influence on groundwater intrusion," *Environmental Earth Sciences*, vol. 75, no. 4, p. 326, 2016.
- [42] J. Ren and X. Ge, "Study of rock meso-damage evolution law and its constitutive model under uniaxial compression loading," *Chinese Journal of Rock Mechanics and Engineering*, vol. 20, no. 4, pp. 425–425, 2001.
- [43] D. Ma, X. X. Miao, Z. Q. Chen, and X. B. Mao, "Experimental investigation of seepage properties of fractured rocks under different confining pressures," *Rock Mechanics and Rock Engineering*, vol. 46, no. 5, pp. 1135–1144, 2013.
- [44] J. Rutqvist and O. Stephansson, "The role of hydromechanical coupling in fractured rock engineering," *Hydrogeology Journal*, vol. 11, no. 1, pp. 7–40, 2003.
- [45] D. T. Snow, "Rock fracture spacings, openings and porosities," *Journal of the Soil Mechanics and Foundations Division*, vol. 94, no. 1, pp. 73–92, 1969.
- [46] L. Zou, L. Jing, and V. Cvetkovic, "Roughness decomposition and nonlinear fluid flow in a single rock fracture," *International Journal of Rock Mechanics and Mining Sciences*, vol. 75, pp. 102–118, 2015.
- [47] Z. S. Chang, Y. S. Zhao, Y. Q. Hu, and D. Yang, "Theoretic and experimental studies on seepage law of single fracture under 3D stresses," *Chinese Journal of Rock Mechanics and Engineering*, vol. 23, no. 4, pp. 620–620, 2004.



Hindawi

Submit your manuscripts at  
[www.hindawi.com](http://www.hindawi.com)

